Pergamon

Acta mater. 49 (2001) 2527–2537

Acta MATERIALIA

www.elsevier.com/locate/actamat

MEAN STRESS EFFECTS ON FLOW LOCALIZATION AND FAILURE IN A BULK METALLIC GLASS

K. M. FLORES and R. H. DAUSKARDT†

Department of Materials Science and Engineering, Stanford University, Stanford, CA 94305-2205, USA

(Received 13 December 2000; received in revised form 15 March 2001; accepted 15 March 2001)

Abstract—The effect of stress state on strain localization and subsequent failure of a bulk metallic glass alloy is examined. It is shown that failure is associated with a critical tensile mean stress of 0.95 GPa. This is in contrast with previous work utilizing superimposed compressive mean stresses, which found that failure resulted at a critical effective stress. Interestingly, the critical tensile mean stress measured in this study causes the same dilatation as a 274 K temperature increase, nearly to the glass transition temperature. The effect of mean stress on elastic variation of the average free volume is added to a strain localization model. This model describes the compressive mean stress behavior very well, and predicts a strong sensitivity to tensile mean stresses. © *2001 Published by Elsevier Science Ltd on behalf of Acta Materialia Inc.*

Keywords: Metallic glasses; Mean stress

1. INTRODUCTION

Bulk metallic glasses have shown potential as structural materials due to their impressive range of mechanical properties [1], although structural applications are currently limited by the lack of any significant plastic deformation. For example, uniaxial tensile strengths of 2 GPa [2] have been reported, but this high strength is accompanied by remarkably little plastic deformation compared to polycrystalline metallic materials with similar properties. Similar to metallic glasses in the form of thin ribbons, bulk metallic glasses fail by forming intense shear bands which propagate catastrophically due to the lack of grain structure and work hardening [2–4]. Early work on the fracture behavior of metallic glasses noted the presence of voids and vein patterns on fracture surfaces [5–8], indicating the activation of flow processes and suggesting that fracture may occur via microvoid coalescence.

The larger dimensions of bulk metallic glass samples make it possible to modify shear band behavior by changing the stress state. This paper describes a study of the effect of stress state on strain localization and subsequent failure in a $Zr_{41.25}Ti_{13.75}Ni_{10}Cu_{12.5}Be_{22.5}$ bulk metallic glass. Unlike previous studies [2, 9] in which superimposed compressive mean stresses were utilized, this work concentrates on stress states with tensile mean stresses. The critical failure stress was measured using a series of notched tensile bars with varying notch radii to examine a range of stress states. A fully plastic Bridgman analysis [10] was initially used to calculate both the stress state and effective plastic strain at failure of notched tensile bars machined from the metallic glass. While changing the notch severity appeared to have little effect on the total plastic strain, the size of the shear band zone was affected, suggesting an effect of stress state on the local plasticity.

The lack of appreciable plastic strain led to the consideration of other possible failure criterion for metallic glasses. Previous work in this area has been inconclusive, with possible yield criterion ranging from a pressure independent von Mises criterion [2, 11] to a normal stress sensitive Mohr–Coulomb criterion [9, 11]. In this work, an elastic analysis based on the work of Neuber [13] led to the conclusion that tensile mean stresses play an important role in the failure of the metallic glass. It is shown that the elastic mean stress developed in the notched bars at failure is sufficient to lower the glass viscosity considerably, in agreement with free volume models for shear band formation [14]. Specifically, a flow model was modified to include the effect of tensile and compressive mean stresses and the resulting catastrophic softening stress was found to be consistent with experimental failure values.

† To whom all correspondence should be addressed. Tel.: +1-650-725-0679; Fax: +1-650-725-4034.

E-mail address: dauskardt@stanford.edu (R. H. Dauskardt)

1359-6454/01/$20.00 © 2001 Published by Elsevier Science Ltd on behalf of Acta Materialia Inc.
PII: S1359-6454(01)00125-2

2. EXPERIMENTAL

The stress-state modified critical fracture strain was measured using a notched tensile bar, illustrated in Fig. 1 [15, 16]. Varying the radius of the notch relative to the diameter of the bar allows a range of stress states to be examined. Under *fully plastic conditions*, Bridgman's analysis [10] of the stress distribution in a necking bar may be used to estimate the stress state parameter, the ratio of the mean stress to the effective stress, at the center of the notched bar:

$$\frac{\sigma_m}{\sigma_{eff}} = \frac{1}{3} + \ln\left(\frac{a}{2\rho} + 1\right) \quad (1)$$

where a is the final minimum bar radius and ρ is the radius of the notch. Note that Bridgman's analysis assumes a von Mises yield criterion and that failure initiates at the center of the bar. The effective plastic strain is given by:

$$\bar{\varepsilon}_\rho = 2 \ln\frac{a_0}{a}, \quad (2)$$

where a_0 is the initial minimum bar radius. The strain is assumed to be constant across the cross section. By varying the notch or bar radii, the stress state may be varied from uniaxial ($a/2\rho \to 0$, $\sigma_m/\sigma_{eff} \to 1/3$) to nearly triaxial ($a/2\rho \to \infty$, $\sigma_m/\sigma_{eff} \to \infty$).

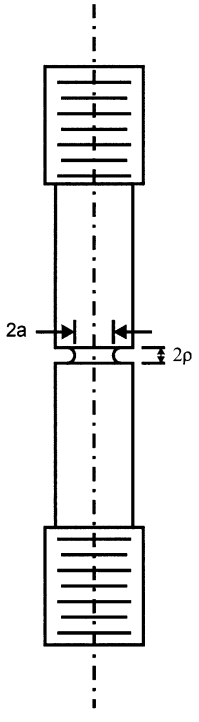

Fig. 1. Schematic illustration of the notched tensile bars used in this study. The notch root radius and diameter of the notched section are indicated.

Notched bars with a 44 mm long, 10 mm diameter gauge section and 2.50 mm notch depth were machined from $Zr_{41.25}Ti_{13.75}Ni_{10}Cu_{12.5}Be_{22.5}$ bulk metallic glass rods (Fig. 1). Relevant material properties for this alloy are given in Table 1. The notch radius was varied between 0.25 and 2.50 mm, with all other dimensions held constant. The round bars were threaded at the ends for attachment to the load frame. Universal joints were utilized at both ends for proper alignment. Testing was performed on an electro-servo-hydraulic system with a crosshead displacement rate of 5 μm/s. This resulted in strain rates in the notch region of $\sim 8\times10^{-5}$ s^{-1}. Elongation across the notch was monitored with an extensometer. The initial and final bar diameters were carefully measured at the notch root for the effective plastic strain calculation (equation (2)).

3. RESULTS

All tensile bars failed at the notch with a cup and cone type morphology similar to that found in ductile metals. A typical failure surface is shown in Fig. 2(a). Fractographic evidence revealed that failure initiated at some point in the interior of the notched region of the bar, rather than at the notch tip. The initiation site is shown at higher magnification in Fig. 2(b,c). The crack front propagated radially on a plane perpendicular to the tensile axis, followed by the formation of ~45° shear lips. Note the appearance of equiaxed voids at the initiation site. There is a significant difference between these voids and the morphology of the rest of the central and shear lip regions, which are shown in Fig. 3. Voids and evidence of local melting are visible in both areas, although the voids have different characteristics. Most notably, voids in the shear lip region are smeared in the direction of shear, and there are several previously molten droplets on the surface.

The variation in effective plastic strain with stress state parameter is shown in Fig. 4(a). A high strength steel is also shown for comparison. Although fractography revealed evidence of plastic flow processes, the metallic glass showed no significant change in effective plastic strain with stress state. In fact, there was almost no measurable plastic strain in any of the bars ($\bar{\varepsilon}_\rho \leq 0.01$). In marked contrast, various ductile crystalline metals exhibit much larger values of $\bar{\varepsilon}_\rho$

Table 1. Relevant material properties for the $Zr_{41.25}Ti_{13.75}Ni_{10}Cu_{12.5}Be_{22.5}$ bulk metallic glass

Material property	Value
Young's modulus, E [22]	96 GPa
Poisson's ratio, ν [22]	0.36
Shear modulus, μ	35.3 GPa
Bulk modulus, B	114.3 GPa
Thermal expansion coefficient, α [22]	10.1×10^{-6} K^{-1}
Glass transition temperature, T_g [23]	625 K
Average atomic volume, Ω	16.4 A^3

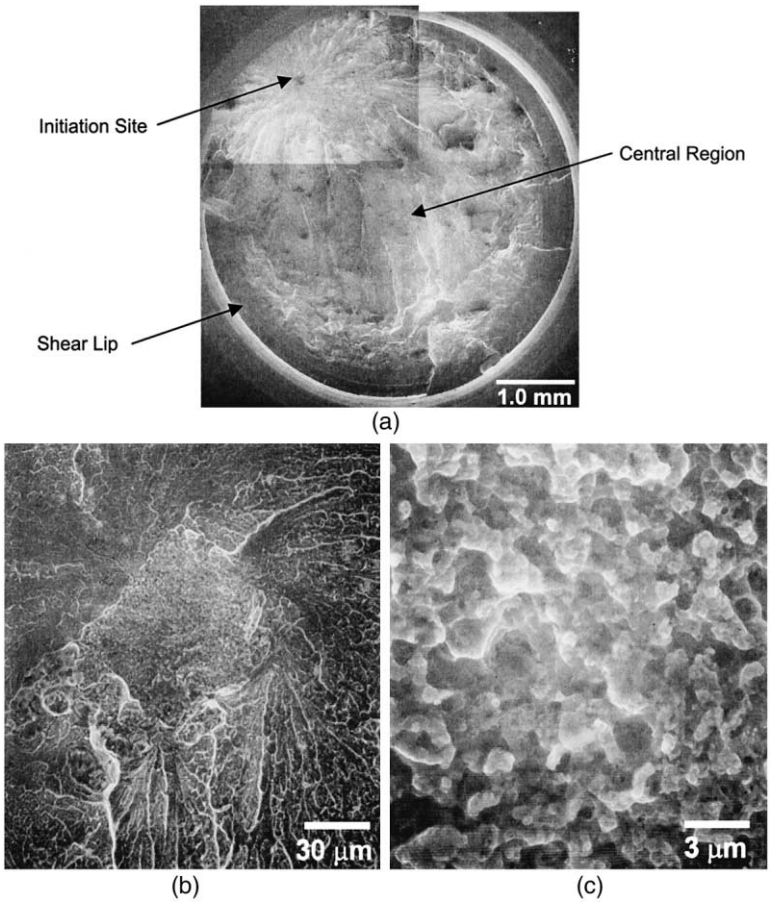

Fig. 2. Micrographs of the failure surface of 1.25 mm notch radius bar. The failure initiation site is clearly visible in the upper left corner of (a), and is shown at higher magnification in (b) and (c). Note the equiaxed voids in (c).

which decrease significantly as the stress state is changed from uniaxial to triaxial [Fig. 4(a)].

On the other hand, a variation in the average strength and the size of the shear lip region with stress state parameter was observed, as shown in Fig. 4(b). The shear lip area ratio was defined as:

$$\text{shear lip area ratio} = \frac{\text{area of shear lip}}{\text{failure cross sectional area}} \quad (3)$$

The failure stress in the notched region decreased from 2.4 to 1.5 GPa with increasing triaxiality. The shear lip area ratio also decreased with increasing triaxiality, and interestingly, the failure stress and the shear lip area ratio appeared to be linearly dependant, as illustrated in Fig. 4(c). Clearly, while both of these properties were sensitive to the notch geometry, the absence of detectable plastic strains suggested that an elastic analysis of the stress state would be more appropriate. As described below, the elastic analysis revealed stress states that are quite similar to the fully plastic Bridgman analysis in the center of the notched region, but differ markedly towards the notch root.

4. ELASTIC ANALYSIS OF NOTCHED TENSILE BARS

We now consider an elastic analysis of the notched region, using the elastic solution for stresses in a notched bar derived by Neuber [13]. We assume that the bar behaves elastically until failure. Neuber assumed a hyperbolic notch and used an ellipsoidal coordinate system, (u, v, w), where a constant u defines an ellipsoid, v defines a hyperboloid, and w defines planes which bisect the bar longitudinally. The hyperboloid $v = v_0$ defines the notch. Using an appropriate coordinate change, these stresses may be expressed in terms of radial and axial coordinates r and z, rather than u and v. Finally, the effective and mean stresses ahead of the notch may be determined after some manipulation and simplification as shown in Appendix A.

Using equations (A9a) and (A9b), it may be shown that the stress state parameter, σ_m/σ_{eff}, is a function of both r and z in addition to the notch root radius. The significant radial variation of the elastic stress state of the bar at the minimum cross section is shown

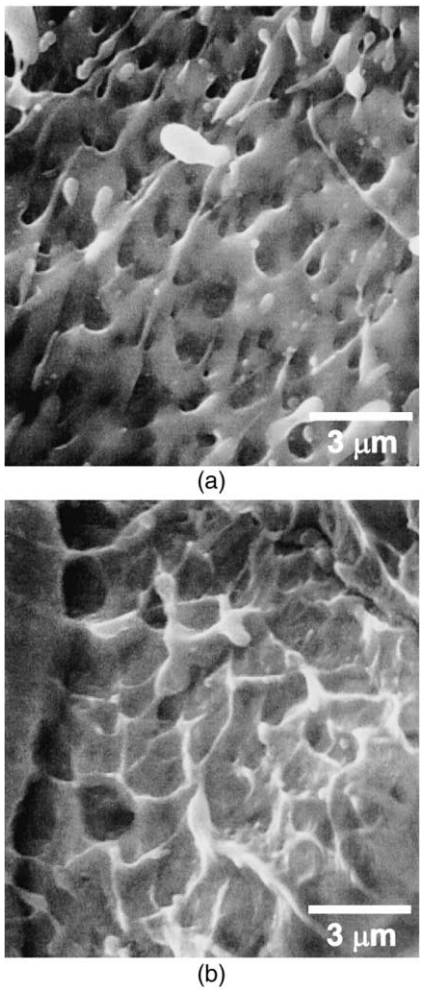

Fig. 3. Micrographs of the failure surface of 0.25 mm notch radius bar with a cup and cone morphology. The void morphologies for the (a) shear and (b) central regions are shown. Note the molten droplets clearly visible in (a).

in Fig. 5(a) for a range of notch radii. In the center of the notched regions, the stress state ranged from more than 3 to less than 0.7 for the notch root radii employed in the present work. The variation in the mean stress is plotted in Fig. 5(b). The mean stress achieves a maximum at the notch root and drops off quickly toward the center of the bar. The effective and maximum shear stresses behave similarly.

No failure criteria was apparent by plotting the failure stress or any appropriate invariant of the stress tensor as a function of the stress state at either the center of the bar or at the notch tip. However, the maximum shear stress at the notch tip varied between 1.25 and 2.25 GPa, larger than the shear yield stress of ~1 GPa noted in other studies [2], suggesting that a small amount of flow may have occurred at the notch tip. Indeed, slight non-linearities in the load–displacement data were noted, although the non-linear longitudinal strain across the notch did not exceed the 0.2% offset definition for yielding. While the shear stresses at the notch tip were quiet high, they fall off quickly towards the center of the bar. Thus any flow was confined to the outer region of the bar. This may have changed the notch geometry slightly, but the effect on the final failure characteristics modeled in this study was expected to be small.

The effective, mean, normal, and maximum shear stresses at the failure initiation site were compared as functions of the stress state at failure as shown in Fig. 6(a). The best fit lines clearly illustrate that only the mean stress at failure remains relatively constant with stress state, with an average value of 0.95±0.13 GPa. This suggests that a critical mean stress is attained at failure for the tensile stress states examined. The fact that failure did not initiate at the notch root, where the mean stress is maximum, is a result of the stochastic nature of failure initiation. The probability of failure initiation at a small inhomogeneity increases as the volume of material sampled increases.

5. DISCUSSION

Previous work [2, 11] has suggested that a von Mises criterion may describe the onset of flow localization and failure for metallic glasses. Alternatively, it is reasonable to expect that the initiation of flow may be controlled by the mean stress or the stress normal to the failure plane, since the shear bands associated with plasticity are areas of increased free volume. Figure 6(b) compares the mean and effective stresses calculated at the failure initiation site with those found in other studies using uniaxial tension, compression, and torsion [2] and compression and tension with superimposed gas pressure [9]. These studies cover a range of stress state parameters from −0.33 to 0.33 (uniaxial compression to uniaxial tension) and suggest that a von Mises based criterion predicts the onset of failure in bulk metallic glass. However, over the stress state parameter range examined in this study, from 0.6 to 1.2 at the failure initiation site, it is apparent that a von Mises criterion is inappropriate, since the effective stress at failure varies markedly with stress state (Fig. 6). Rather, it would appear that a failure criterion involving the mean stress ought to apply since the mean stress at the failure initiation site remains constant with stress state. The average mean stress at this position is ~0.95 GPa, 42% greater than the maximum mean stress obtained in the other studies. It is also notable that the effective stresses in this study quickly drop below the average effective stress found in the other studies.

Other studies have noted an effect of tensile versus compressive loading on the angle of the failure plane. Lowhapandu *et al*. [9] measured very little change in failure strength between tensile and compressive loading, but did measure a considerable angle change. Failure occurred at ~42° (with respect to the loading axis) in compression, ~57° in tension with superimposed gas pressure, and ~90° in pure uniaxial tension. However, in their study of a Zr–Al– Ti–Cu–Ni bulk

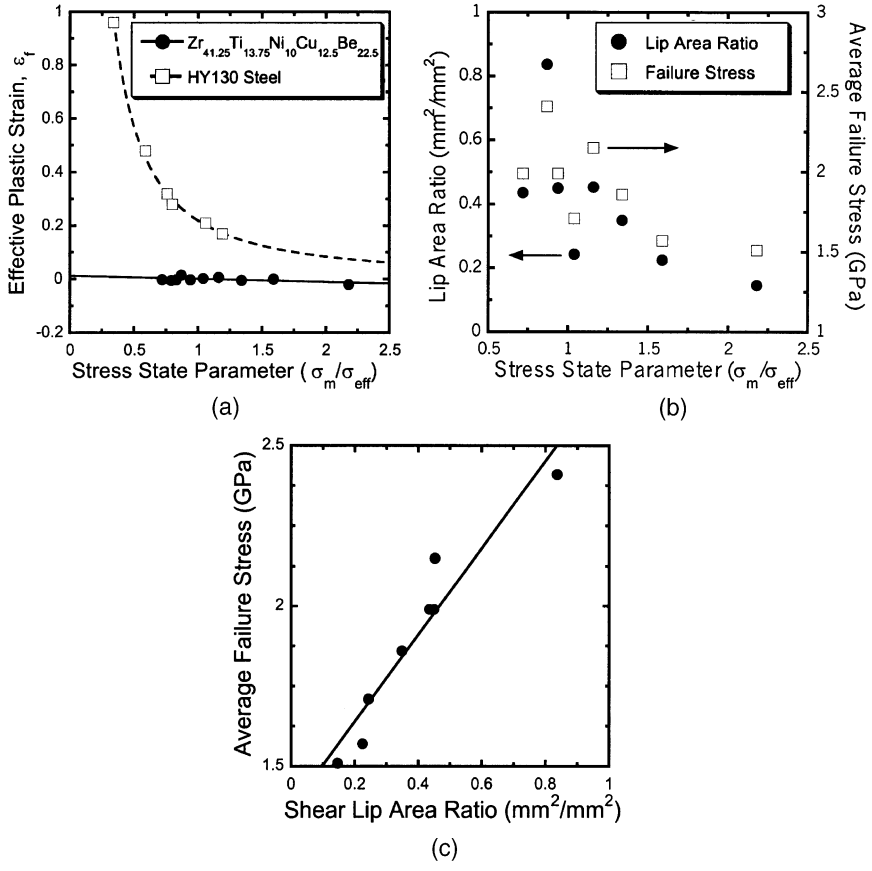

Fig. 4. (a) The variation of effective plastic strain with stress state. The results for a pressure vessel steel are shown for comparison [15]. (b) The variation of failure stress and shear lip area ratio with stress state. Failure stress and shear lip area ratio are shown to be linearly dependant in (c).

metallic glass, Liu *et al.* [4] determined that compressive failure occurred at 45°, on the plane of maximum shear, while tensile failure occurred at a smaller axial stress at ~54° to the loading axis. Both studies attribute the angle change to a sensitivity to normal stresses, described by the Mohr–Coulomb criterion:

$$\tau = k_1 - k_2\sigma_n, \tag{4}$$

where τ and σ_n are the shear and normal stresses on the failure plane, respectively, and k_1 and k_2 are constants. The hypothesis is that, although plastic flow is the result of a shear stress driven diffusive process, a tensile stress normal to the shear plane causes a local free volume increase, aiding diffusion. In this study, a linear relationship between the normal and shear stresses was not observed. Failure initiated on a plane perpendicular to the loading axis, where the shear stress τ was everywhere equal to 0. This suggests that equation (4), with its dependence on the stresses acting on the failure plane, is not applicable in its present form for this alloy. However, the local value of the mean stress is shown below to have a significant effect on the flow behavior.

Following the example of Spaepen [17] and Steif *et al.* [18], we examine the effect of mean stresses on the flow localization stress in metallic glasses. For applied shear stresses sufficiently large such that the free volume creation rate is greater than the annihilation rate, the net rate of change of the free volume, v_f, is given by [18]:

$$\dot{v}_f = v^* f \exp\left[-\frac{\Delta G^m}{kT}\right]\exp\left[-\frac{\alpha_g v^*}{v_f}\right] \times\left[\frac{2\alpha_g kT}{v_f S}\left(\cosh\frac{\tau\Omega}{2kT}-1\right)-\frac{1}{n_D}\right] \tag{5}$$

where v^* is the critical free volume required for an atomic jump (~0.8 Ω); n_D is the number of jumps required to annihilate v^*; ΔG^m is the activation energy for an atomic jump; τ is the applied shear stress; Ω is the atomic volume; f is the jump frequency; k is Boltzman's constant; T is the temperature; α_g is a geometrical factor on the order of 1; S is a material constant given by $\frac{2}{3}\mu\frac{1+\nu}{1-\nu}$; ν is Poisson's Ratio; and μ is the shear modulus. Within the shear band, we assume that the metallic glass behaves homo-

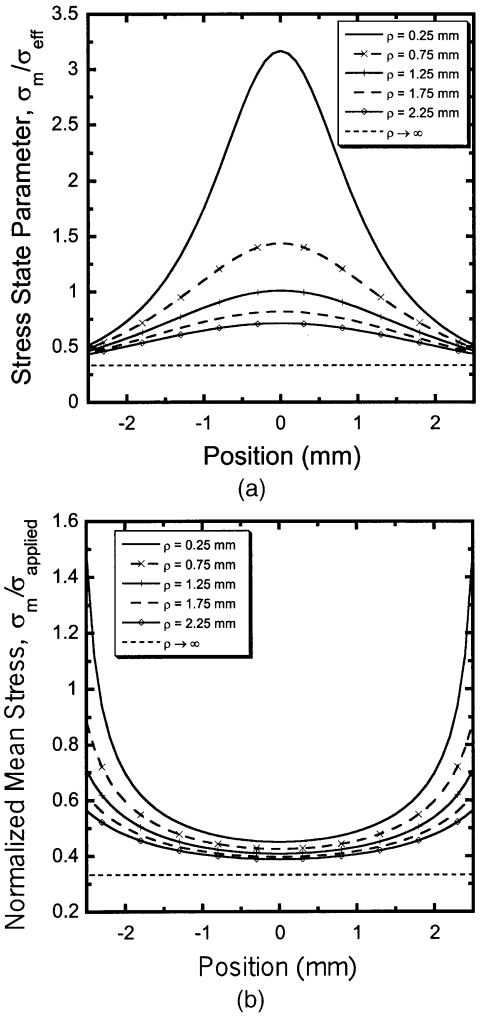

Fig. 5. The variation in stress state parameter (a) and mean stress (b) across a 5 mm diameter bar for a range of notch radii, based on the Neuber solution for the elastic stresses in a notched bar.

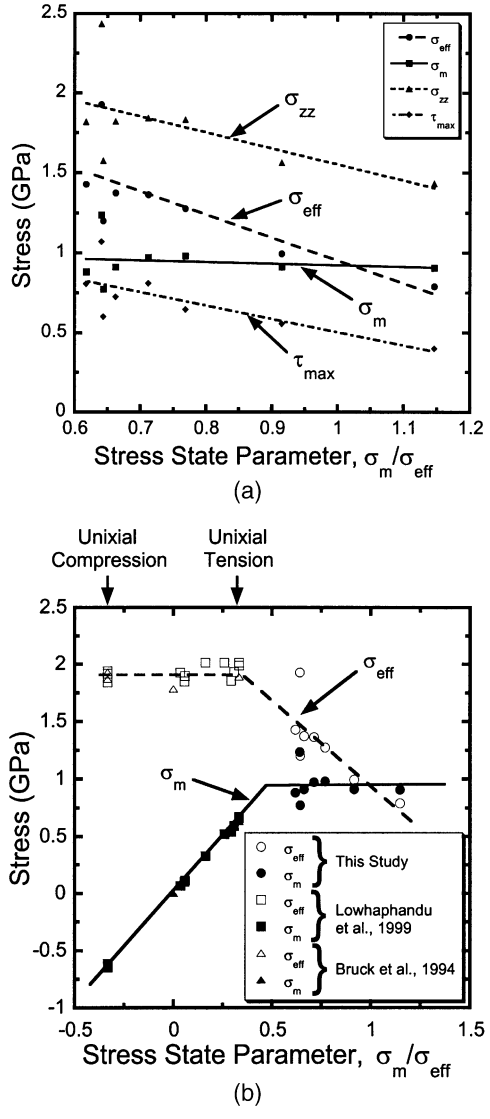

Fig. 6. The effective, mean, normal and maximum shear stresses at the initiation site are plotted as a function of stress state in (a). The effective and mean stresses are compared with those found in other studies in (b) [2, 9].

geneously. For a solid undergoing homogeneous shearing,

$$\dot{\gamma} = \frac{\dot{\tau}}{\mu} + 2f \exp\left[-\frac{\alpha_g v^*}{v_f}\right] \exp\left[-\frac{\Delta G^m}{kT}\right] \sinh\left[\frac{\tau\Omega}{2kT}\right] \quad (6)$$

where $\dot{\gamma}$ is the (constant) strain rate, and $\dot{\tau}$ is the rate of change of the applied stress [18].

We now modify Spaepen and Steif *et al.*'s work to include the effect of superimposed compressive and tensile mean stresses. We assume that the sole effect of the mean stress is to increase or decrease the initial free volume, v_i. Equations (5) and (6) are then solved numerically with the initial conditions $\tau(t = 0) = 0$ and $v_f(t = 0) = v_i$. There are two extreme cases for the variation of initial free volume with mean stress. In one case, the dilatation of the free volume is taken to be the same as the elastic dilatation of the material as a whole. That is, the atomic (hard sphere) volume itself changes under the application of the mean stress. In this case, the initial free volume is given by:

$$v_i = v_0\left(1 + \frac{\sigma_m}{B}\right) \quad (7a)$$

where v_0 is the initial free volume with no superimposed mean stress and B is the bulk modulus. This is a reasonable expression for compressive mean stresses where the electron orbits uniformly contract, thus decreasing the size of the atom as well as the free volume sites as suggested by Cohen and Turnbull [19]. At the other extreme, all of the dilatation is attri-

buted to a change in free volume, and the hard sphere atomic volume is held constant:

$$v_i = v_0 + \Omega\frac{\sigma_m}{B} \tag{7b}$$

Note that equation (7b) only gives sensible results for tensile mean stresses. For even relatively small compressive mean stresses, equation (7b) indicates that the initial free volume becomes negative. We therefore only apply equation (7b) for stress states greater than zero. Note also that equation (7b) describes a much larger free volume change for a given increment of mean stress than is the case with equation (7a), since v_0 is only a small fraction of Ω.

Solving equations (5) and (6) for representative values of unstressed initial free volume, mean stress, and strain rate results in the constitutive behavior illustrated in Fig. 7 where equation (7a) is used for compressive mean stresses and equation (7b) for tensile mean stresses. The expressions are nondimensionalized, following Steif's example [18]. The initially linear elastic shear stress–strain behavior is followed by a catastrophic softening associated with a dramatic increase in free volume and the localization of strain in shear bands. For large strains, the model predicts a steady state stress and free volume.

As expected, the stress–strain behavior is altered markedly for small superimposed tensile mean stresses, while small compressive mean stresses have a much smaller effect. Tensile mean stresses cause a significant drop in the shear stress required for softening, while compressive mean stresses lead to a slight increase. The steady state values also decrease under tensile mean stresses, although they appear unaffected by compressive mean stresses. In fact, for large enough tensile mean stresses, the maxima approaches the steady state plateau, and the catastrophic nature of the softening is lost. Additionally, the free volume immediately after the mean stress is applied approaches the steady state value.

Steif *et al.* [18] derived a closed form expression to approximate the softening stress resulting from equations (5) and (6). This approximation assumes that the material behaves elastically to the abrupt softening stress and neglects free volume annihilation. It does, however, require a minimum stress, $\tau_0>0$, for free volume creation. For small initial free volumes ($<10\%$), Steif's analysis results in an expression of the form:

$$\begin{aligned}&\alpha_g\dot{\gamma}\left[f\exp\left(-\frac{\Delta G_m}{2kT}\right)\right]^{-1} \\ &\times\left(\frac{\mu\Omega}{2kT}\right)\left(\frac{Sv^*}{2kT}\right)\left(\frac{v_i}{\alpha_g v^*}\right)^3\exp\left(\frac{\alpha_g v^*}{v_i}\right) \\ &= (1+\Lambda)\sinh\frac{\tau_{max}\Omega}{2kT} - \frac{\tau_{max}\Omega}{2kT} - \left(\sinh\frac{\tau_0\Omega}{2kT} - \frac{\tau_0\Omega}{2kT}\right)\end{aligned} \tag{8}$$

where Λ and τ_0 are defined in [20]. Using equations (7a) and (7b) to describe the initial free volume as a function of the mean stress, we now have an expression for the relationship between the mean stress and the softening stress for the metallic glass.

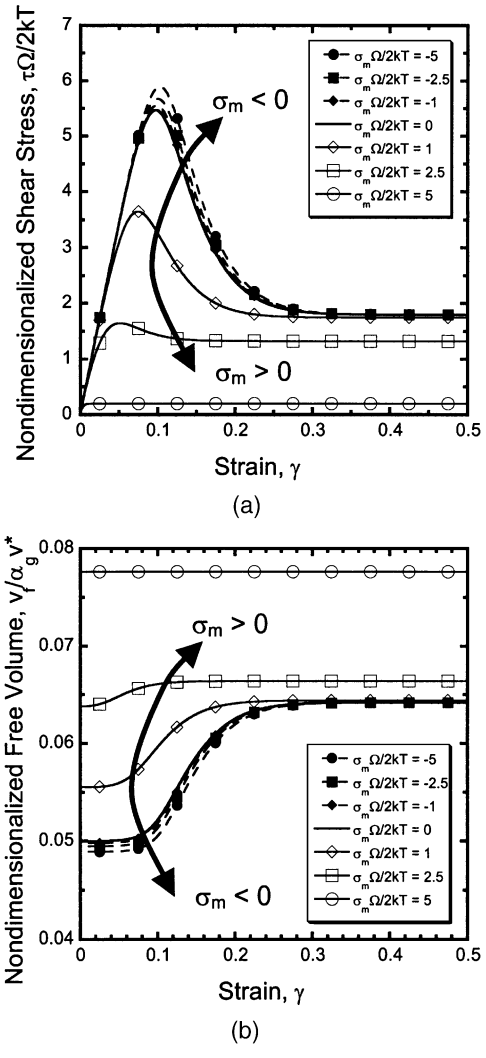

Fig. 7. The nondimensionalized stress–strain behavior of a metallic glass is shown for a range of nondimensionalized mean stresses in (a). The corresponding behavior of the nondimensionalized free volume is shown in (b). The unstressed initial free volume $v_0/\alpha_g v^* = 0.05$, $n_D = 3$, and the nondimensionalized strain rate $\dot{\gamma}(f\exp[-\Delta G^m/kT])^{-1} = 10^{-6}$. The initial free volume is described by equation (7a) for compressive mean stresses, equation (7b) for tensile mean stresses.

The maximum shear stress found from equation (8) and the superimposed mean stress are used to calculate the stress state parameter at the onset of softening, and the variation in the mean and effective stresses with stress state is shown in Fig. 8. Using the initial, unstressed free volume, the nondimensionalized strain rate, and the number of jumps required to annihilate the free volume as fitting parameters, we obtain excellent agreement between this model and the data for superimposed mean stresses, also shown in Fig. 8. The behavior for stress states less than 1/3

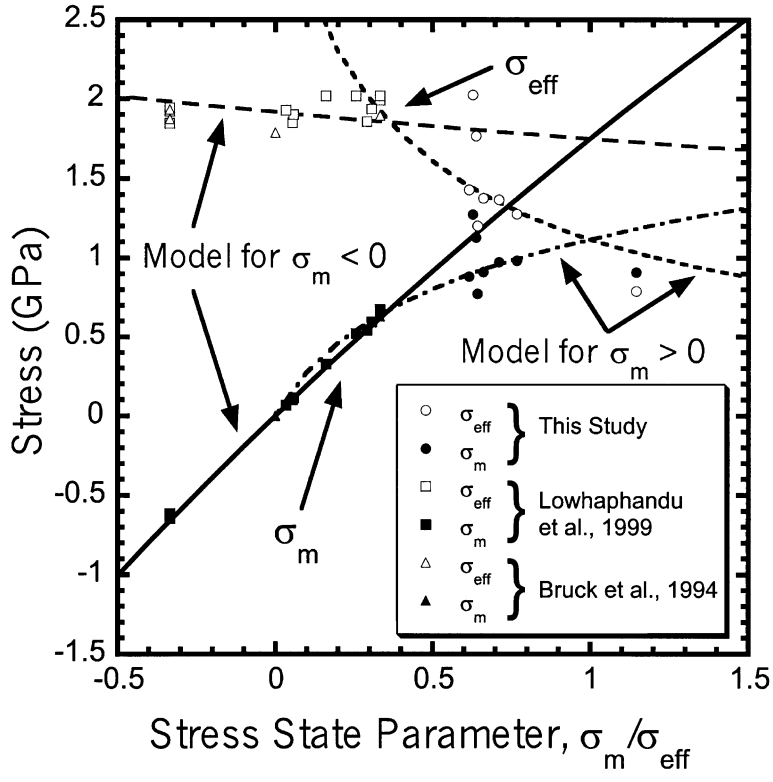

Fig. 8. Correlation between the free volume model presented in this study and the mean and effective stresses measured for a range of stress states. The unstressed initial free volume $v_0/\alpha_g v^*$ used in the free volume model is 0.062 for equation (7a) and 0.055 for equation (7b), n_D is 3, and the nondimensionalized strain rate $\dot{\gamma}(f \exp[-\Delta G^m/kT])^{-1} = 10^{-6}$.

(uniaxial tension) is described very well by the free volume model, using equation (7a) for the variation in initial free volume with mean stress. Thus, flow localization in the bulk metallic glass under superimposed compressive mean stresses may be explained by a catastrophic increase in the free volume at a characteristic softening stress.

The modified flow model with equation (7b) describing the tensile mean stress effect on the catastrophic softening stress is consistent with trends in experimental failure values for stress states greater than 0 (Fig. 8). The mean stress for shear localization initially increases with stress state, but quickly begins to flatten out for larger stress state parameters. Note that in our experimental work, a constant mean stress was not superimposed, as we implicitly assume in the modified flow model. Rather, the mean and effective stresses were both functions of the applied uniaxial load and therefore increased during the course of the experiment. Failure for tensile stress states occurred at a critical mean stress value, before the peak effective stress associated with catastrophic softening was necessarily reached. The model and data do suggest, however, that the free volume in the metallic glass is indeed more sensitive to tensile than compressive mean stresses.

The cross over from the behavior described by equation (7a) to the critical mean stress at failure more closely described by equation (7b) also suggests a transition in final failure mode following initiation of flow. The critical tensile mean stress value and the fractographic evidence of equiaxed voids at the failure initiation site [Fig. 2(c)] are indications that final failure involved void formation and growth. Initial flow and subsequent void formation most likely occurred in the vicinity of a small flaw or inhomogeneity where the stresses were locally increased. As the voids grew and coalesced into a larger flaw, unstable fracture occurred, giving rise to the river markings radiating away from the failure initiation site.

In the model presented in this study, large mean stresses directly change the free volume and thus the glass viscosity. Since the glass transition temperature is the temperature at which the viscosity reaches a specific level (~10^{12} Pa s), we may also say that mean stresses cause a shift in T_g. Samwer *et al.* [20] have examined the effect of hydrostatic pressure on the T_g, of an alloy similar to the one used in this study. They cooled the alloy from the melt under hydrostatic pressure, annealed at that pressure well below T_g and then performed a DSC scan at ambient pressure. The study measured a slight increase in T_g with pressure of about 3.6 K/GPa, associated with subtle atomic rearrangements during the anneal. Although the glass transition temperature was not actually determined at high pressure, the relatively small effect of hydro-

static pressure during the anneal is consistent with the small effect of compressive stresses on the localization stress found in this study [equation (7a)].

To get a sense of the relative importance of the change in free volume associated with mean stresses, Spaepen [14] compared the dilatation associated with crack tip stresses with that associated with thermal expansion between room and the glass transition temperature. The dilatation due to an applied mean stress is given by:

$$\frac{\Delta V}{V} = \frac{\sigma_m}{B}. \tag{9}$$

Setting this equal to the dilatation due to thermal expansion,

$$\frac{\Delta V}{V} = 3\alpha\Delta T, \tag{10}$$

the temperature change which causes the same dilatation as the applied mean stress may be computed:

$$\Delta T = \frac{\sigma_m}{3\alpha B}. \tag{11}$$

With the material properties given in Table 1, a mean stress of 0.95 GPa causes a dilatation equivalent to increasing the temperature by 274 K, to about 51 K below the glass transition temperature of 625 K. In the vicinity of a small flaw or inhomogeneity in the material, the local mean stress would be even higher, further increasing the dilatation and the effective temperature rise. While temperature has additional effects on the kinetics of flow, this order of magnitude estimate suggests that the critical mean stress would be sufficient to lower the viscosity of the metallic glass, giving rise to the obviously softened appearance of the fracture surface. Once the final fracture process has begun, localized heating on the order of tens of degrees [21] would lower the viscosity further, even to the point of leaving molten droplets on the fracture surface.

6. CONCLUSIONS

Although the failure surface of the notched bars exhibited void patterns and obvious softening, no significant plastic strains were measured in the $Zr_{41.25}Ti_{13.75}Ni_{10}Cu_{12.5}Be_{22.5}$ bulk metallic glass. However, the size of the shear lip region increased linearly with the average failure stress, suggesting that the notch severity and thus the stress state do have an effect on failure. An elastic analysis of the bars revealed that the mean stress calculated at the failure initiation site was relatively constant, although the effective stress and therefore the stress state parameter at this position varied. This suggested that a critical mean stress was necessary to cause fracture over the range of stress states studied. Equiaxed voids were observed at the initiation site, consistent with the presence of large tensile mean stresses contributing to the deformation. The constant mean stress observed in this work is contrasted with the constant effective stress seen over a different stress state parameter range used in other studies.

The effect of both tensile and compressive mean stresses on the free volume and thus the yielding behavior of the metallic glasses was modeled. Compressive mean stresses caused a slight increase in the localization stress, while the effect of tensile mean stresses on the free volume and thus the localization stress was much more pronounced. The asymmetry in the free volume change under tensile and compressive mean stresses is notable. Previous studies of the effect of mean stress have concentrated only on compression, and found the effect to be small. This work confirms this marginal effect of compressive mean stress on flow localization but shows that it is still consistent with the free volume model for flow. We further demonstrate that the free volume is much more sensitive to tensile mean stresses, consistent with the observed constant tensile mean stress at failure.

Acknowledgements—Materials used in this study were provided by Amorphous Technologies International, Laguna Nigel, California. This work was supported by the Air Force Office of Scientific Research under AFOSR Grant No. F49620-98-1-0260.

REFERENCES

1. Johnson, W. L. and Peker, A., in *Science and Technology of Rapid Solidification and Processing*, ed. M. A. Otooni. Kluwer, Dordrecht, 1995, p. 25.
2. Bruck, H. A. *et al.*, *Scripta metall.*, 1994, **30**, 429.
3. Bruck, H. A., Rosakis, A. J. and Johnson, W. L., *J. Mater. Res.*, 1996, **11**, 503.
4. Liu, C. T. *et al.*, *Met. Trans. A*, 1998, **29A**, 1811.
5. Leamy, H. J., Chen, H. S. and Wang, T. T., *Met. Trans.*, 1972, **3**, 699.
6. Spaepen, F., *Acta metall.*, 1975, **23**, 615.
7. Pampillo, C. A. and Reimschuessel, A. C., *J. Mater. Sci.*, 1974, **9**, 718.
8. Pampillo, C. A. and Chen, H. S., *Mater. Sci. Eng.*, 1974, **13**, 181.
9. Lowhaphandu, P., Montgomery, S. L. and Lewandowski, J. J., *Scripta mater.*, 1999, **41**, 19.
10. Bridgman, P. W., *Studies in Large Plastic Flow and Fracture*. Harvard University Press, Cambridge, MA, 1964.
11. Kimura, H. and Masumoto, T., in *Amorphous Metallic Alloys*, ed. F. E. Luborsky. Butterworth, London, 1983, p. 187.
12. Donovan, P. E., *Acta metall.*, 1989, **37**, 445.
13. Neuber, H., *Theory of Notch Stresses*. Edwards Brothers Inc, Ann Arbor, MI, 1946.
14. Spaepen, F. and Turnbull, D., *Scripta Metal.*, 1974, **8**, 563.
15. Mackenzie, A. C., Hancock, J. W. and Brown, D. K., *Eng. Fract. Mech.*, 1977, **9**, 167.
16. Hancock, J. W. and Mackenzie, A. C., *J. Mech. Phys. Solids*, 1976, **24**, 147.

17. Spaepen, F., *Acta metall.*, 1977, **25**, 407.
18. Steif, P. S., Spaepen, F. and Hutchinson, J. W., *Acta metall.*, 1982, **30**, 447.
19. Cohen, M. H. and Turnbull, D., *J. Chem. Phys.*, 1959, **31**, 1164.
20. Samwer, K., Busch, R. and Johnson, W. L., *Phys. Rev. Let.*, 1999, **82**, 580.
21. Flores, K. M. and Dauskardt, R. H., *J. Mater. Res.*, 1999, **14**, 638.
22. Conner, R. D. *et al., Scripta mater.*, 1997, **37**, 1373.
23. Peker, A. and Johnson, W. L., *Appl. Phys. Let.*, 1993, **63**, 2342.

APPENDIX A

Application of Neuber's analytical expression for the elastic stresses in a notched bar is not trivial and details are reproduced here for completeness. Neuber [13] employed ellipsoidal coordinates (u, v, w) to solve the problem of elastic stresses in a circumferentially notched bar, as illustrated in Fig. A1. The ellipsoidal coordinates are sets of confocal ellipses and hyperbolae, rotated in the w direction about the longitudinal axis of the bar. The set of hyperbolae are described by:

$$\left(\frac{r}{c\,\sin v}\right)^2-\left(\frac{z}{c\,\cos v}\right)^2=1. \tag{A1a}$$

Similarly, the set of ellipses are described by:

$$\left(\frac{r}{c\,\cosh u}\right)^2+\left(\frac{z}{c\,\sinh u}\right)^2=1. \tag{A1b}$$

In equations (A1a) and (A1b), the constant c is the radial distance to the common focus of the hyperbolae and ellipses. In order to have the tip of the semicircular notch coincide with the tip of the hyperbola $v=v_0$ used in Neuber's analysis, c is defined as:

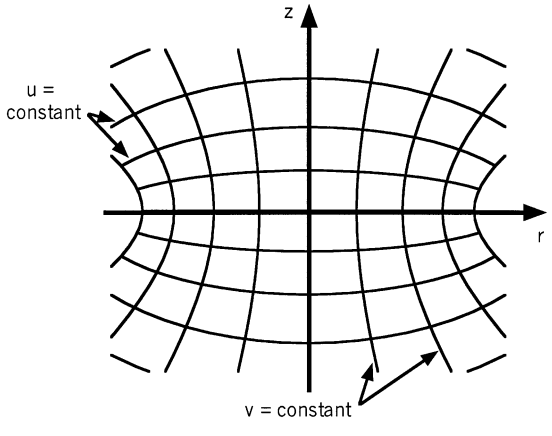

Fig. A1. The elliptical coordinate system used in Neuber's derivation of the elastic stress field in a notched tensile bar is illustrated. Lines of constant u are ellipses, while lines of constant v are hyperbolae. The coordinate w represents a rotation about the longitudinal z axis.

$$c=\sqrt{a(a+\rho)} \tag{A2}$$

where a is the minimum radius of the bar and ρ is the radius of the notch. Note that at the notch tip, $r=a$, $z=0$, and $v=v_0$. Equations (A1a) and (A2) may then be used to relate the hyperbolic notch to known geometric parameters:

$$\sin v_0=\sqrt{\frac{a}{a+\rho}}, \tag{A3a}$$

and therefore

$$\cos v_0=\sqrt{\frac{\rho}{a+\rho}}. \tag{A3b}$$

Neuber's analysis results in the following stresses in ellipsoidal coordinates:

$$\sigma_{uu}=\frac{1}{h^2}\left[A\tanh^2 u+B\frac{\cos v}{\cosh^2 u}+C\left(-2-\alpha+\frac{1}{\cosh^2 u}\right)\cos v\right]+\frac{\cos v}{h^4}(-A+B+C\cos^2 v) \tag{A4a}$$

$$\sigma_w=\frac{1}{h^2}\left[-A\frac{\cos v}{1+\cos v}+C(\alpha-1)\cos v\right]+\frac{\cos v}{h^4}(A-B-C\cos^2 v) \tag{A4b}$$

$$\sigma_{ww}=\frac{1}{h^2}\left[A\left(-\tanh^2 u+\frac{\cos v}{1+\cos v}\right)-B\frac{\cos v}{\cosh^2 u}+C\left(\alpha-1-\frac{1}{\cosh^2 u}\right)\cos v\right] \tag{A4c}$$

$$\sigma_{uv}=-\frac{\tanh u\,\sin v}{h^2}\left[-\frac{A}{1+\cos v}+C(\alpha-1)+\frac{1}{h^2}(-A+B+C\cos^2 v)\right] \tag{A4d}$$

Neuber initially uses a Cartesian coordinate system to describe generalized deformation, later switching to the curvilinear (u, v, w) coordinates more appropriate for the hyperbolic notch. The *factor of distortion*, h, accounts for the distortion encountered when transferring from the Cartesian system to the ellipsoidal system, and is given by:

$$h=\sqrt{\sinh^2 u+\cos^2 v} \tag{A5}$$

Note that $u = 0$ corresponds to the plane of the minimum cross section, and that σ_{vv} at $u = 0$ is the stress in the direction of the loading axis, i.e. $\sigma_{vv} = \sigma_{zz}$ at $u = 0$. The constants A, B, and C are determined from boundary conditions to be:

$$A = C(\alpha-1)(1 + \cos v_0) \tag{A6a}$$

$$B = A - C\cos^2 v_0 \tag{A6b}$$

$$C = -\frac{\sigma_{avg}}{2}\frac{1 + \cos v_0}{1 + (2-\alpha)\cos v_0 + \cos^2 v_0}, \tag{A6c}$$

where σ_{avg} is the average longitudinal stress in the minimum cross section and $\cos v_0$ is given by equation (A3b) above. The constant α is related to Poisson's ratio:

$$\alpha = 2(1-\nu). \tag{A7}$$

Finally, in this analysis it is more convenient to calculate the stress field in terms of radial coordinates (r, θ, z). We may use equations (A1a) and (A1b) to express u, v, and w in terms of r, θ, and z:

$$u = \sinh^{-1}\left\{\sqrt{\frac{1}{2}[(r^2 + z^2 - 1) + \sqrt{(1-r^2-z^2)^2 + 4z^2}]}\right\} \tag{A8a}$$

$$v = \cos^{-1}\left\{\sqrt{\frac{1}{2}[-(r^2 + z^2 - 1) + \sqrt{(1-r^2-z^2)^2 - 4r^2}]}\right\} \tag{A8b}$$

and

$$w = \theta \tag{A8c}$$

from which the radial stress components can be determined. Note that to calculate invarients of the stress tensor, it was not necessary to convert the stresses themselves to the radial coordinate system. The resulting effective and mean stresses ahead of the notch tip are given by:

$$\sigma_{eff}(r,z) = \left[\left(\frac{\sigma_{uu}(r,z)-\sigma_{vv}(r,z)}{2}\right)^2 + \left(\frac{\sigma_{uu}(r,z)-\sigma_{ww}(r,z)}{2}\right)^2 + \left(\frac{\sigma_{vv}(r,z)-\sigma_{ww}(r,z)}{2}\right)^2 - 3(\sigma_{uv}(r,z))^2\right]^{1/2} \tag{A9a}$$

and

$$\sigma_m(r,z) = \frac{1}{3}(\sigma_{uu}(r,z) + \sigma_{vv}(r,z) + \sigma_{ww}(r,z)). \tag{A9b}$$